electronic reprint

Journal of
Applied Crystallography
ISSN 0021-8898
Editor: **Gernot Kostorz**

Small-angle neutron scattering resolution with refractive optics

Boualem Hammouda and David F. R. Mildner

Journal of
Applied Crystallography
ISSN 0021-8898

Received 29 October 2006
Accepted 26 December 2006

Small-angle neutron scattering resolution with refractive optics

Boualem Hammouda* and David F. R. Mildner

National Institute of Standards and Technology, Center for Neutron Research, 100 Bureau Drive, Gaithersburg, MD 20899-8562, USA. Correspondence e-mail: hammouda@nist.gov

The resolution of small-angle neutron scattering instruments is investigated for the case where refractive optics (lenses or prisms) are used. The appropriate equations are derived to describe the position and the spatial variance of the neutron beam at the detector in the horizontal and vertical directions, and the minimum value of the scattering vector. This is given for the spectrometer without any additional optics, and with the insertion of converging lenses or prisms. The addition of the lenses decreases the sample-aperture contribution to the resolution to enable an increase of neutron current at the sample. They also reduce the size of the penumbra of the beam at the detector, thereby lowering the minimum value of the scattering vector. The prisms correct the effect of gravity on the vertical beam position, and make the beam spot less asymmetric.

1. Introduction

Small-angle neutron scattering (SANS) is a valuable method for materials characterization, probing structures from the near atomic level to the near micrometre size scale. SANS has found ever growing use in many areas of research, including polymers, complex fluids, biology, materials science, magnetism and condensed matter physics. The resolution of conventional SANS instruments has been modeled and is well understood (Mildner & Carpenter, 1984). Demand for increased neutron current and better resolution has led to the use of neutron focusing methods using refractive lenses (Choi *et al.*, 2000; Eskildsen *et al.*, 1998; Mildner *et al.*, 2005). The use of long-wavelength neutrons is hampered by resolution smearing due to gravity. Refractive prisms have been used to correct for gravity effects (Forgan & Cubitt, 1998).

The goal here is to present the theoretical basis for the SANS resolution when refractive optics (in the form of lenses and/or prisms) are used. Measurements of SANS resolution are also included together with comparison of calculated and measured resolution parameters, such as the neutron beam size characteristics at the detector. The focus here will be on the standard deviation of the SANS instrumental resolution function and on the minimum scattering variable (so-called minimum-Q). These two figures of merit are important in the performance of SANS instruments. The neutron beam current on the sample as measured by the area detector is also included.

SANS resolution is discussed for circular-aperture collimation in the following three cases: (i) the empty-beam case (where no lenses and no prisms are in the beam), (ii) the case with focusing lenses inserted, and (iii) the case where gravity-correcting refractive prisms are placed immediately before the sample aperture.

2. SANS resolution function

The SANS resolution function is often represented by a peaked Gaussian function of standard deviation σ_Q, where Q is the scattering variable given by $Q = (4\pi/\lambda)\sin(\theta/2)$. Here θ is the scattering angle and λ is the neutron wavelength. For all practical purposes, in the small-angle range $Q \simeq 2\pi\theta/\lambda$. The one-dimensional convolution smearing integral (suitable for measurements that are azimuthally symmetric) is given by

$$\frac{\mathrm{d}\Sigma(Q_x)}{\mathrm{d}\Omega} = \int_{-\infty}^{+\infty} \mathrm{d}Q'_x P_{1\mathrm{D}}(Q'_x) \frac{\mathrm{d}\Sigma(|Q_x - Q'_x|)}{\mathrm{d}\Omega}. \quad (1)$$

Here the one-dimensional resolution function is defined as

$$P_{1\mathrm{D}}(Q'_x) = \left(\frac{1}{2\pi\sigma^2_{Q'_x}}\right)^{1/2} \exp\left(-\frac{Q'^2_x}{2\sigma^2_{Q'_x}}\right). \quad (2)$$

The two-dimensional version (suitable for measurements that are azimuthally asymmetric) is given by

$$\frac{\mathrm{d}\Sigma(Q,\varphi)}{\mathrm{d}\Omega} = \int_0^{+\infty} Q' \mathrm{d}Q' P_{2\mathrm{D}}(Q') \times \int_0^{2\pi} \mathrm{d}\varphi \frac{\mathrm{d}\Sigma\left([Q^2 + Q'^2 - 2QQ'\cos(\varphi)]^{1/2}, \varphi\right)}{\mathrm{d}\Omega} \quad (3)$$

and

$$P_{2\mathrm{D}}(Q') = \left(\frac{1}{\pi\sigma^2_{Q'}}\right) \exp\left(-\frac{Q'^2}{\sigma^2_{Q'}}\right). \quad (4)$$

Here φ is the polar angle between scattering vectors $\mathbf{Q}$ and $\mathbf{Q}'$. Note that when the x and y components are equivalent (azimuthally symmetric scattering and symmetric resolution

function) the one-dimensional version is simpler because it involves a single integration and can be used on radially averaged SANS data. The one-dimensional and the two-dimensional Q variances are related by $\sigma_Q^2 = \sigma_{Q_x}^2 + \sigma_{Q_y}^2$ since $Q^2 = Q_x^2 + Q_y^2$. The Q standard deviation σ_Q is related to the spatial standard deviation (*i.e.* standard deviation of the neutron beam spot at the detector) σ_r by $\sigma_Q = (2\pi/\lambda L_2)\sigma_r$, where L_2 is the sample-to-detector distance.

3. Standard SANS configuration

The first (and simplest) case considered corresponds to an empty-beam configuration (with no lenses and no prisms) in the beam.

3.1. Standard deviation

In the 'standard' SANS optics configuration (with no lenses and no prisms), the variance of the Q resolution has two main contributions: one due to the neutron 'wavelength spread' and one due to the instrument configuration 'geometry' (Mildner & Carpenter, 1984):

$$\sigma_Q^2 = (\sigma_Q^2)_{\rm wav} + (\sigma_Q^2)_{\rm geo} = Q^2\frac{\sigma_\lambda^2}{\lambda^2} + \left(\frac{2\pi}{\lambda}\right)^2\frac{\sigma_r^2}{L_2^2}. \qquad (5)$$

This result was obtained assuming that there is no correlation between wavelength and geometry. Here $\sigma_\lambda^2 = \langle\lambda^2\rangle - \langle\lambda\rangle^2$ is the variance of the wavelength distribution. Assuming a triangular wavelength distribution of full width at half-maximum (FWHM) $\Delta\lambda$, for which $\sigma_\lambda^2/\lambda^2 = (1/6)(\Delta\lambda/\lambda)^2$, the neutron 'wavelength spread' contribution is given by

$$(\sigma_Q^2)_{\rm wav} = Q^2\frac{1}{6}\left(\frac{\Delta\lambda}{\lambda}\right)^2. \qquad (6)$$

For the instrument configuration 'geometry' part, we will focus on the spatial variance σ_r^2 which has components in the horizontal and vertical directions ($\sigma_r^2 = \sigma_x^2 + \sigma_y^2$). The contribution in the horizontal direction is given by

$$(\sigma_x^2)_{\rm geo} = \left(\frac{L_2}{L_1}\right)^2\frac{R_1^2}{4} + \left(\frac{L_1+L_2}{L_1}\right)^2\frac{R_2^2}{4} + \frac{1}{3}\left(\frac{\Delta x_3}{2}\right)^2. \qquad (7)$$

L_1 and L_2 are the source-to-sample and sample-to-detector distances, respectively, R_1 and R_2 are the source and sample circular-aperture radii, respectively, and Δx_3 is the horizontal size of the detector cell. A uniformly illuminated source aperture has been assumed. The instrument-geometry contribution in the vertical direction σ_y^2 is similar except for the last term, which becomes $(1/3)(\Delta y_3/2)^2$. The 'geometry' part of the Q resolution σ_Q is obtained from the spatial resolution σ_r as $\sigma_Q = (2\pi/\lambda L_2)\sigma_r$.

The final contribution to the resolution is due to the effect of gravity on the neutron trajectories. Neutron trajectories follow a parabola in the vertical plane:

$$y = y_0 - A\lambda^2 \quad \text{with} \quad A = L_2(L_1+L_2)\frac{gm^2}{2h^2}. \qquad (8)$$

Here g is the gravitation constant ($g = 9.81$ m s^{-2}), m is the neutron mass and h is Planck's constant ($h/m = 3995$ Å m s^{-1}). The constant $A = 3.073 \times 10^{-7}L_2(L_1 + L_2)$ is given in units of m Å^{-2}.

The effect of gravity adds the following contribution to the variance of the spatial resolution:

$$(\sigma_y^2)_{\rm grav} = A^2(\langle\lambda^4\rangle - \langle\lambda^2\rangle^2) = A^2\lambda^4\frac{2}{3}\left(\frac{\Delta\lambda}{\lambda}\right)^2. \qquad (9)$$

The last expression was obtained for a triangular wavelength distribution.

In summary, the variance of the Q resolution is obtained by putting together all terms:

$$\begin{aligned}
\sigma_Q^2 &= \sigma_{Q_x}^2 + \sigma_{Q_y}^2,\\
\sigma_{Q_x}^2 &= \left(\frac{2\pi}{\lambda}\right)^2\frac{\sigma_x^2}{L_2^2} + Q_x^2\frac{1}{6}\left(\frac{\Delta\lambda}{\lambda}\right)^2,\\
\sigma_{Q_y}^2 &= \left(\frac{2\pi}{\lambda}\right)^2\frac{\sigma_y^2}{L_2^2} + Q_y^2\frac{1}{6}\left(\frac{\Delta\lambda}{\lambda}\right)^2,\\
\sigma_x^2 &= \left(\frac{L_2}{L_1}\right)^2\frac{R_1^2}{4} + \left(\frac{L_1+L_2}{L_1}\right)^2\frac{R_2^2}{4} + \frac{1}{3}\left(\frac{\Delta x_3}{2}\right)^2,\\
\sigma_y^2 &= \left(\frac{L_2}{L_1}\right)^2\frac{R_1^2}{4} + \left(\frac{L_1+L_2}{L_1}\right)^2\frac{R_2^2}{4} + \frac{1}{3}\left(\frac{\Delta y_3}{2}\right)^2\\
&\quad + A^2\lambda^4\frac{2}{3}\left(\frac{\Delta\lambda}{\lambda}\right)^2. \qquad (10)
\end{aligned}$$

These equations have been derived before (Mildner & Carpenter, 1984; Mildner *et al.*, 2005). They have been included here for the sake of completeness.

3.2. Minimum beam spot size

A figure of merit of SANS instruments is the minimum value of the scattering variable (also called $Q_{\rm min}$) that can be reached for a given configuration. This value is imposed by the neutron spot size on the area detector, which in turn dictates the size of the beamstop to be used. In order to minimize the spot size, one has to minimize the 'umbra' and 'penumbra' of the neutron beam at the detector.

Given the standard SANS geometry, the extent of the penumbra in the horizontal direction is given by

$$X_{\rm min} = \frac{L_2}{L_1}R_1 + \frac{L_1+L_2}{L_1}R_2 + \frac{\Delta x_3}{2}, \qquad (11)$$

and the minimum Q in the horizontal direction is therefore $Q_{\rm min}^X = (2\pi/\lambda)(X_{\rm min}/L_2)$.

In the vertical direction, the effect of gravity plays a role. The upper edge of the penumbra moves down by $A(\lambda - \Delta\lambda)^2$ because it corresponds to faster neutrons with wavelength $\lambda - \Delta\lambda$. The lower edge of the penumbra drops down by more; *i.e.* by $A(\lambda + \Delta\lambda)^2$ because it corresponds to slower neutrons with wavelength $\lambda + \Delta\lambda$. This results in an oval (not elliptical) beam spot at the detector. To first order in wavelength spread, one obtains

$$Y_{\min} = \frac{L_2}{L_1}R_1 + \frac{L_1 + L_2}{L_1}R_2 + \frac{\Delta y_3}{2} + 2A\lambda^2\left(\frac{\Delta\lambda}{\lambda}\right). \quad (12)$$

In practice, $Q_{\min}$ is determined by the spot size in the vertical direction where the beam is the broadest, $Q_{\min} = Q^Y_{\min} = (2\pi/\lambda)(Y_{\min}/L_2)$:

$$Q_{\min} = \left(\frac{2\pi}{\lambda L_2}\right)\left[\frac{L_2}{L_1}R_1 + \frac{L_1 + L_2}{L_1}R_2 + \frac{\Delta y_3}{2} + 2A\lambda^2\left(\frac{\Delta\lambda}{\lambda}\right)\right]. \quad (13)$$

A specific instrument configuration is considered next.

3.3. Instrument configuration

Consider the following instrument configuration corresponding to the 30 m NG3 SANS instrument (Glinka *et al.*, 1998) at the NIST Center for Neutron Research (NCNR):

$$\begin{aligned} L_1 &= 16.14 \text{ m}, \\ L_2 &= 13.19 \text{ m}, \\ R_1 &= 0.715 \text{ cm}, \\ R_2 &= 0.635 \text{ cm}, \\ \Delta x_3 &= \Delta y_3 = 0.5 \text{ cm}, \\ \frac{\Delta\lambda}{\lambda} &= 0.13. \end{aligned} \quad (14)$$

This gives $A = 0.01189$ cm Å^{-2}. The neutron wavelength λ is 6 Å. The configuration does not strictly obey the 'cone rule' whereby the beam spot umbra at the detector is eliminated.

Fig. 1 shows the variance σ_Q^2 of the Q resolution for increasing scattering variable Q.

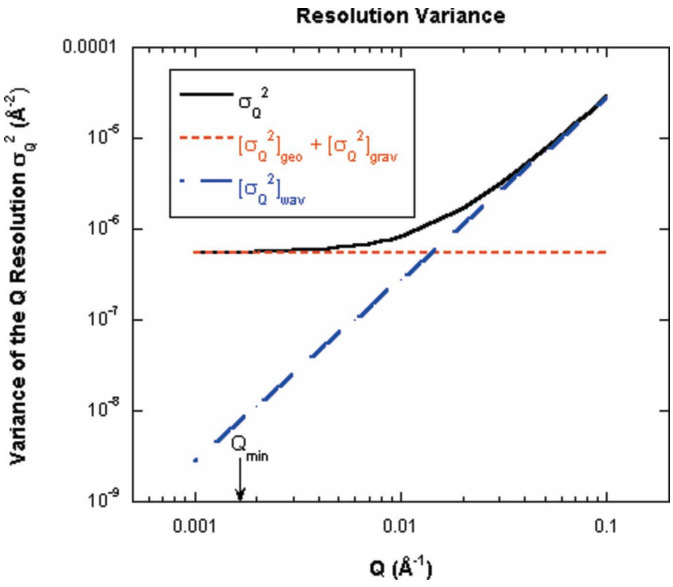

Figure 1
Variation of σ_Q^2 with Q plotted on a log–log scale. The two main contributions (geometry and wavelength spread) are added in quadrature. Gravity effects are small for the wavelength considered here (λ = 6 Å).

$$\begin{aligned} \sigma_Q^2 &= 5.55 \times 10^{-7} + 0.00282Q^2 \text{ (Å}^{-2}\text{)} \\ Q_{\min} &= 0.00167 \text{ Å}^{-1}. \end{aligned} \quad (15)$$

Gravity effects are small for 6 Å neutrons. Neutrons fall by only 0.428 cm.

The focus here will be on empty-beam measurement (*i.e.* with no sample in the beam). This corresponds to the resolution limit of $Q = 0$ throughout.

3.4. Empty-beam measurements

Measurements were made using the above instrument configuration and varying the neutron wavelength. Using the equations developed in the previous sections, measurements obtained on the NG3 30 m SANS instrument at the NIST CNR are compared with predictions.

Fig. 2 shows the standard deviations σ_x and σ_y of the neutron spot size with increasing neutron wavelength. The measured values were obtained by performing non-linear least-squares fits to a Gaussian function in the x and in the y directions. Fits were performed on cuts through the beam spot center, both horizontally and vertically. Data recorded by two adjacent detector cells (normal to the cut) were added in each case in order to improve statistics. A scaling factor of $1.45^{1/2} = 1.2$ was used to scale the measured data. This scaling factor gave good agreement between the measured and calculated values for σ_x. The same scaling factor was used for σ_y.

This necessary scaling factor of 1.2 is probably related to the procedure used to obtain measured beam spot widths. (i) Slice cuts were performed in the horizontal and vertical directions. (ii) Moreover, Gaussian fits were performed on these slices even though the beam profile is known to be of a trapezoidal shape (not Gaussian). (iii) Lastly, the measured beam spots

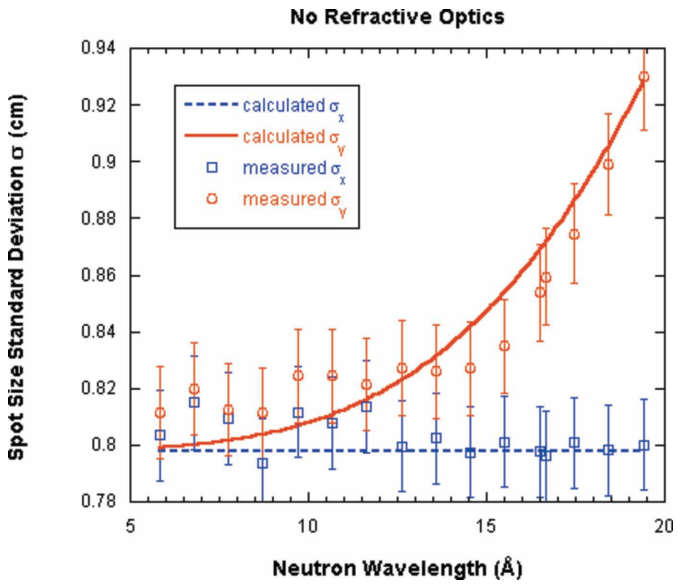

Figure 2
Variation of the measured and calculated neutron spot-size standard deviations σ_x and σ_y with increasing wavelength. Statistical error bars (obtained from the fits) have been included.

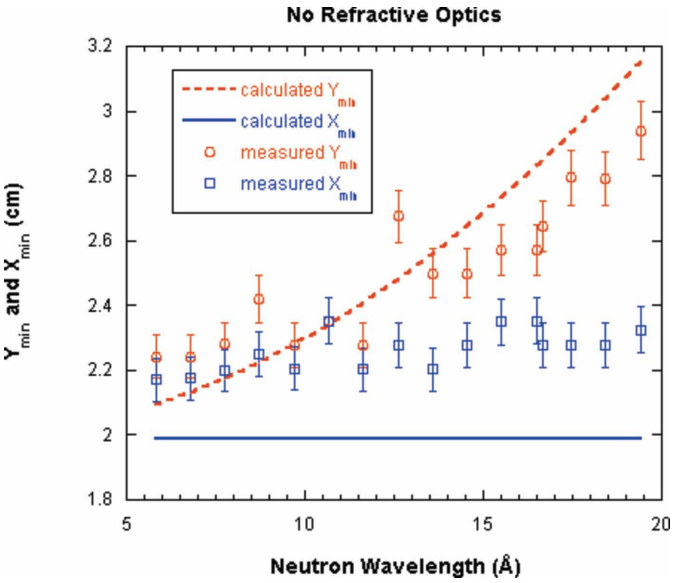

Figure 3
Variation of the neutron beam spot sizes in the horizontal and vertical directions with increasing wavelength. Statistical errors have been included. The measured spot sizes are overestimated.

were so small (covering only a few detector cells) that Gaussian fits were performed with four to eight points only.

Fig. 3 shows the minimum spot sizes $X_{\min}$ and $Y_{\min}$ obtained experimentally as the values where the intensity (of the horizontal or vertical cuts across the beam spot) goes to zero. This method is conservative and overestimates the measured values for $X_{\min}$. It is not precise, yielding poor agreement between measured and calculated values. Our calculated values neglect for instance diffuse scattering from the beam-defining sample aperture and from the pre-sample and post-sample neutron windows. Such scattering tends to broaden the neutron beam. At long wavelengths the gravity effect broadens the neutron spot in the vertical direction with the extra difference $Y_{\min} - X_{\min}$ given by the term $2A\lambda^2(\Delta\lambda/\lambda)$.

4. Neutron optics using focusing lenses

Biconcave lenses are used to focus the neutron beam. This enhances the neutron current on the sample and yields a lower $Q_{\min}$ by decreasing the neutron beam penumbra. The basic equations for the focusing lens system are reviewed in Appendix *A*. The effect of focusing lenses on the SANS resolution and on $Q_{\min}$ are investigated next.

4.1. Resolution with focusing lenses

Consider a neutron beam with a triangular wavelength distribution and a focusing lens system optimized for the principal wavelength $\bar{\lambda}$ in that distribution. The main focal length is denoted f_0 and corresponds to object-to-lenses and lenses-to-image distances of L_1 and L_2, respectively. Since the source aperture is at the object position, the lenses are at the sample position and the detector is at the image position. L_1 and L_2 are also the source-to-sample and sample-to-detector distances. Now consider another wavelength λ within the same distribution and its corresponding focal length f. The object-to-lenses and lenses-to-image distances are L_1 and L_4, respectively, for this wavelength.

$$\frac{1}{f_0} = \frac{1}{L_1} + \frac{1}{L_2}$$
$$\frac{1}{f} = \frac{1}{L_1} + \frac{1}{L_4}. \tag{16}$$

When lenses are used, the 'geometry' contribution to the SANS resolution becomes

$$\sigma_x^2 = \left(\frac{L_2}{L_4}\right)^2 \frac{R_4^2}{4} + \left(\frac{L_4 - L_2}{L_4}\right)^2 \frac{R_2^2}{4} + \frac{1}{3}\left(\frac{\Delta x_3}{2}\right)^2, \tag{17}$$

where R_4 is the radius of the image of the source aperture for the focal length f at wavelength λ. From the focusing equations and with $f \simeq 1/\lambda^2$ (see Appendix *A*), one obtains

$$\frac{1}{f_0} - \frac{1}{f} = \frac{1}{L_2} - \frac{1}{L_4} = \frac{L_4 - L_2}{L_2 L_4} = \frac{1}{f_0}\left[1 - \left(\frac{\lambda}{\lambda_0}\right)^2\right]. \tag{18}$$

Therefore, after replacing $1/f_0$, one obtains

$$\sigma_x^2 = \left(\frac{L_2}{L_1}\right)^2 \frac{R_1^2}{4} + \left(\frac{L_1 + L_2}{L_1}\right)^2 \left[1 - \left(\frac{\lambda}{\lambda_0}\right)^2\right]^2 \frac{R_2^2}{4} + \frac{1}{3}\left(\frac{\Delta x_3}{2}\right)^2. \tag{19}$$

This is the result valid for any wavelength λ. Around the focal wavelength λ_0, the averaging over the wavelength distribution yields for the squared term $[1 - (\lambda/\lambda_0)^2]^2$ the result $(2/3)(\Delta\lambda/\lambda_0)^2$.

The following result is valid only close to λ_0:

$$\sigma_x^2 = \left(\frac{L_2}{L_1}\right)^2 \frac{R_1^2}{4} + \left(\frac{L_1 + L_2}{L_1}\right)^2 \frac{2}{3}\left(\frac{\Delta\lambda}{\lambda_0}\right)^2 \frac{R_2^2}{4} + \frac{1}{3}\left(\frac{\Delta x_3}{2}\right)^2. \tag{20}$$

Note that the term $(\Delta\lambda/\lambda_0)^2$ makes the second (sample aperture) term very small. This allows the opening up of the sample aperture (*i.e.* by making R_2 large) without much penalty in resolution.

The effect of gravity on the SANS resolution with focusing lenses is the same as without lenses. The result close to λ_0 is

$$\sigma_y^2 = \left(\frac{L_2}{L_1}\right)^2 \frac{R_1^2}{4} + \left(\frac{L_1 + L_2}{L_1}\right)^2 \frac{2}{3}\left(\frac{\Delta\lambda}{\lambda}\right)^2 \frac{R_2^2}{4} + \frac{1}{3}\left(\frac{\Delta y_3}{2}\right)^2 + A^2\lambda^4 \frac{2}{3}\left(\frac{\Delta\lambda}{\lambda}\right)^2. \tag{21}$$

Moreover, the wavelength-spread contribution also remains the same as before:

$$\sigma_{Q_x}^2 = \left(\frac{2\pi}{\lambda}\right)^2 \frac{\sigma_x^2}{L_2^2} + Q_x^2 \frac{1}{6}\left(\frac{\Delta\lambda}{\lambda}\right)^2,$$
$$\sigma_{Q_y}^2 = \left(\frac{2\pi}{\lambda}\right)^2 \frac{\sigma_y^2}{L_2^2} + Q_y^2 \frac{1}{6}\left(\frac{\Delta\lambda}{\lambda}\right)^2. \tag{22}$$

4.2. Minimum Q with focusing lenses

Using the same argument as before, the minimum beam spot sizes in the horizontal and vertical directions are obtained (for each wavelength λ) as

$$X_{\min}(\lambda) = \frac{L_2}{L_1}R_1 + \left(\frac{L_1 + L_2}{L_1}\right)\left|1 - \left(\frac{\lambda}{\lambda_0}\right)^2\right|R_2 + \frac{\Delta x_3}{2} \quad (23)$$

and

$$Y_{\min}(\lambda) = \frac{L_2}{L_1}R_1 + \left(\frac{L_1 + L_2}{L_1}\right)\left|1 - \left(\frac{\lambda}{\lambda_0}\right)^2\right|R_2 + \frac{\Delta y_3}{2} + 2A\lambda^2\left(\frac{\Delta\lambda}{\lambda}\right). \quad (24)$$

Around the focal wavelength λ_0, the minimum spot size is proportional to

$$\left|\left[1 - \left(\frac{\lambda_0 + \Delta\lambda}{\lambda_0}\right)^2\right] - \left[1 - \left(\frac{\lambda_0}{\lambda_0}\right)^2\right]\right| \simeq 2\left(\frac{\Delta\lambda}{\lambda_0}\right)$$

so that the term $|1 - (\lambda/\lambda_0)^2|$ contributes a factor $2(\Delta\lambda/\lambda)$ around λ_0.

The corresponding values of the minimum Q are: $Q^X_{\min} = (2\pi/\lambda)(X_{\min}/L_2)$ and $Q^Y_{\min} = (2\pi/\lambda)(Y_{\min}/L_2)$.

4.3. Measurements with focusing lenses

Neutron optics measurements were made using the same SANS instrument configuration as before, but with a set of seven consecutive biconcave MgF_2 lenses (described in Appendix A) inserted in the beam just before the sample aperture. This set corresponds to a focal wavelength λ_0 around 17.36 Å.

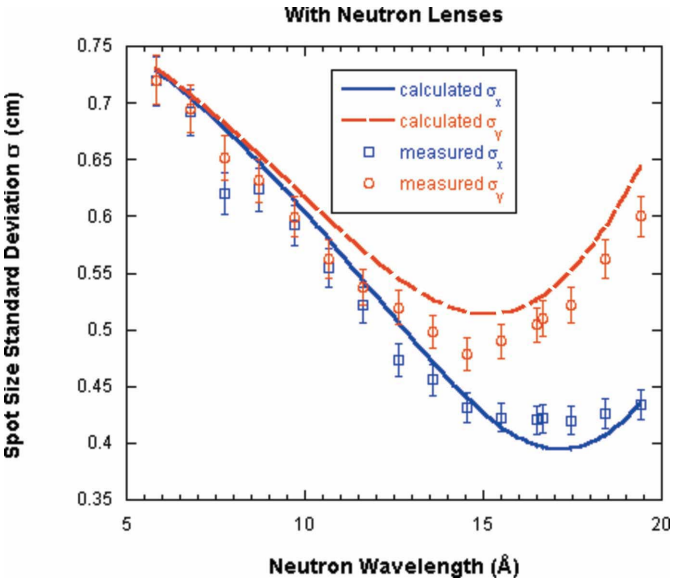

Figure 4
Variation of the spot-size standard deviation with wavelength in the horizontal and vertical directions. The calculated trends agree with the measured ones. Statistical error bars have been included.

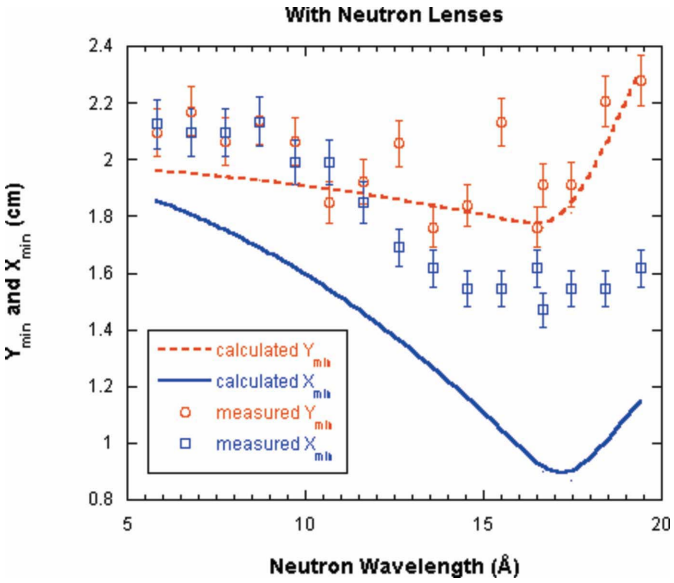

Figure 5
Variation of the minimum spot sizes with increasing wavelength. Statistical errors have been included. The measured spot sizes are overestimated.

Fig. 4 shows that the beam spot resolution has strong (parabolic) wavelength dependence both in the x and in the y direction. The minimum resolution in the horizontal direction corresponds to a focal wavelength λ_0. The minimum in the x direction (λ_0 = 17.2 Å) is taken to be the focal wavelength for our focusing arrangement. The x direction is independent of gravity effects. The same procedure as before was used to obtain these results (including the $1.45^{1/2}$ scaling discussed previously). The calculated trends agree with the measured ones.

Fig. 5 shows the minimum horizontal and vertical spot sizes as a function of increasing wavelength. Here also there is a minimum around λ_0 = 17.2 Å in the x direction and the measured values have been chosen conservatively (as described before) and are found to be overestimates that are higher than the calculated values.

4.4. Discussion

For the sake of consistency and in order to compare the cases with and without lenses, the same configuration was used in both cases (without and with lenses). It should be noted however, that the use of converging lenses has the advantage of allowing the opening up of the sample aperture (*i.e.* increasing R_2) without penalty in resolution. This happens because the penumbra is minimized when lenses are used. The main effect is increased neutron current on the sample.

Refractive lenses are characterized by chromatic aberrations that show up as a dependence of both the variance σ_x^2 and $X_{\min}$ on λ. In order to reduce these chromatic aberrations, $(\Delta\lambda/\lambda)$ could be made smaller, which would result in a penalty in neutron current on the sample.

5. Neutron optics using gravity-correcting prisms

Prisms may be used to deflect the neutron beam upward, thereby correcting for the effect of gravity particularly at long wavelengths and reducing the vertical size of the beam at the detector. The basic prisms equations are included in Appendix *B*.

5.1. Contribution to the *Q* resolution

Within the prism's minimum deflection approximation (Sears, 1989), the variance of the neutron spot size at the detector (where $z = L_1 + L_2$) involves the variance σ_y^2,

$$\sigma_y^2 = (\sigma_y^2)_{\rm geo} + \langle y(L_1 + L_2)^2\rangle - \langle y(L_1 + L_2)\rangle^2, \qquad (25)$$

where

$$y(L_1 + L_2) = -B\lambda^2 L_2(L_1 + L_2) + \delta(\lambda)L_2, \quad z = L_1 + L_2, \qquad (26)$$

where $B = gm^2/2h^2$. With the deviation angle given by $\delta(\lambda) = C\lambda^2$, where C depends on the prism material and apex angle (see Appendix *B*) the following result is obtained:

$$\sigma_y^2 = (\sigma_y^2)_{\rm geo} + (A - L_2C)^2(\langle\lambda^4\rangle - \langle\lambda^2\rangle^2). \qquad (27)$$

Here the gravity variable $A = BL_2(L_1 + L_2)$ has been used. Assuming a triangular wavelength distribution, the wavelength averages are calculated as follows:

$$(\langle\lambda^4\rangle - \langle\lambda^2\rangle^2) = \lambda^4\frac{2}{3}\left(\frac{\Delta\lambda}{\lambda}\right)^2. \qquad (28)$$

Therefore

$$\sigma_y^2 = (\sigma_y^2)_{\rm geo} + (A - L_2C)^2\lambda^4\frac{2}{3}\left(\frac{\Delta\lambda}{\lambda}\right)^2. \qquad (29)$$

This is the variance of the neutron spot spatial resolution at the detector in the vertical direction. The familiar 'geometry' contribution is the same as for the case without prisms. The final result for both directions is therefore given by

$$\sigma_x^2 = \left(\frac{L_2}{L_1}\right)^2\frac{R_1^2}{4} + \left(\frac{L_1 + L_2}{L_1}\right)^2\frac{R_2^2}{4} + \frac{1}{3}\left(\frac{\Delta x_3}{2}\right)^2$$
$$\sigma_y^2 = \left(\frac{L_2}{L_1}\right)^2\frac{R_1^2}{4} + \left(\frac{L_1 + L_2}{L_1}\right)^2\frac{R_2^2}{4} + \frac{1}{3}\left(\frac{\Delta y_3}{2}\right)^2 + (A - L_2C)^2\lambda^4\frac{2}{3}\left(\frac{\Delta\lambda}{\lambda}\right)^2 \qquad (30)$$

The standard deviations of the Q resolution σ_{Q_x} and σ_{Q_y} are obtained by multiplying the spot size standard deviations σ_x and σ_y by the factor $(2\pi/\lambda L_2)$.

5.2. Contribution to $Q_{\rm min}$

$Q_{\rm min}$ has contributions from geometry, the gravity effect and the addition of a prism.

$$Y_{\rm min} = (Y_{\rm min})_{\rm geo} + |A - L_2C|\frac{\left[(\lambda + \Delta\lambda)^2 - (\lambda - \Delta\lambda)^2\right]}{2}. \qquad (31)$$

The wavelength term can be expressed (to first order) as

$$\frac{\left[(\lambda + \Delta\lambda)^2 - (\lambda - \Delta\lambda)^2\right]}{2} \simeq 2\lambda^2\left(\frac{\Delta\lambda}{\lambda}\right). \qquad (32)$$

Therefore

$$Y_{\rm min} = \frac{L_2}{L_1}{\rm R}_1 + \frac{L_1 + L_2}{L_1}R_2 + \frac{\Delta y_3}{2} + |A - L_2C|2\lambda^2\left(\frac{\Delta\lambda}{\lambda}\right). \qquad (33)$$

Note that the same factor $|A - L_2C|$ enters both in the beam spot resolution variance σ_y^2 and in $Y_{\rm min}$. $Q_{y_{\rm min}}$ is obtained by multiplying $Y_{\rm min}$ by the factor $(2\pi/\lambda L_2)$.

5.3. Measurements with correcting prisms

A set of neutron optics measurements have been performed using the instrument configuration described before. Fig. 6 shows a prism cassette containing a row of five prisms used in these measurements. Each prism is made from single-crystal MgF_2 and has a base of 3 × 3 cm and a height of 0.5 cm. In order to correct fully for the effect of gravity, between one and two prism cassettes would have to be used. Here only one cassette is used for the sake of simplicity and in order to test the resolution equations developed here.

The prism angle is equal to $\alpha = 2\tan^{-1}(1.5/0.5) = 143.13^\circ$. The prism variable is $C = 4.896 \times 10^{-6}$ Å^{-2}, yielding an estimate for the factor $L_2C = 6.458 \times 10^{-3}$ cm Å^{-2} and for the factor $|A - L_2C| = 0.00543$ cm Å^{-2}.

Fig. 7 shows the horizontal and vertical beam measured spot positions as a function of wavelength compared with the calculated values. The case with no prisms has been added in order to appreciate the upward deflection introduced by the prisms. The value corresponding to λ = 6 Å has been subtracted in each case for simplicity.

The variance of the neutron beam spot at the detector has also been measured in each case and compared with the calculated value. Fig. 8 shows the square root of the difference in the variances of the beam spot in the orthogonal directions as a function of wavelength. The measured values are obtained using the same procedure described before (taking horizontal and vertical slice cuts across the neutron beam spot). The

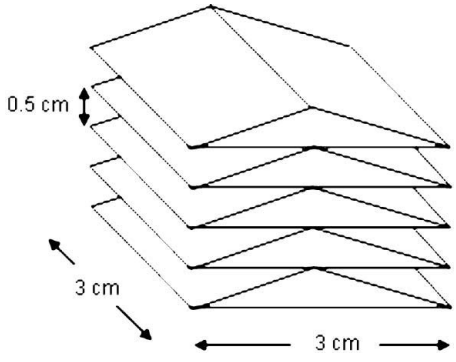

Figure 6
Representation of the prism cassette containing a row of five MgF_2 prisms.

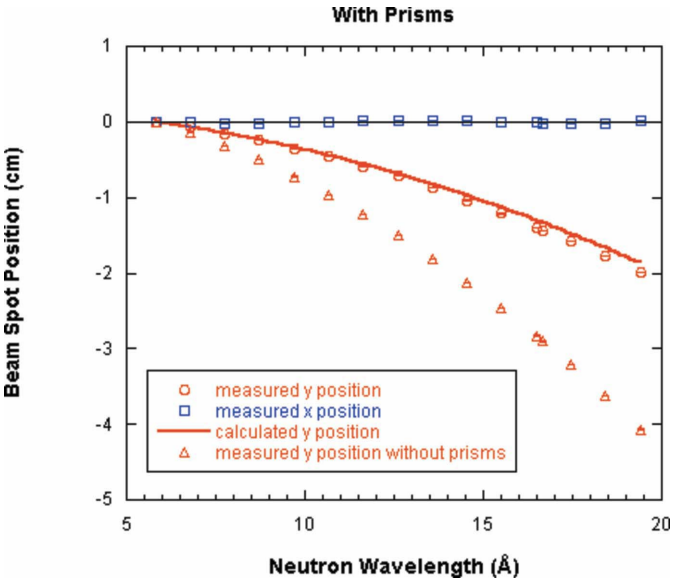

Figure 7
Variation of the neutron beam spot positions with wavelength. Statistical error bars are smaller than the plotting symbols.

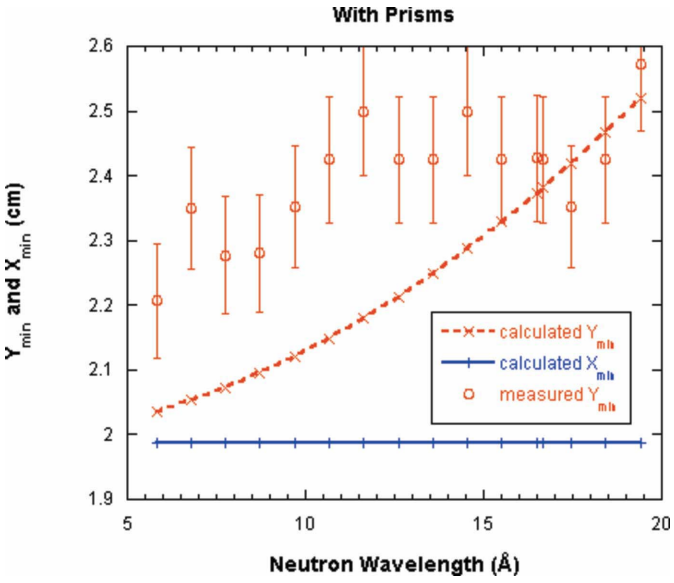

Figure 9
Variation of the minimum spot sizes with increasing neutron wavelength. Statistical errors have been included.

prediction for the case without prisms is also shown. The measured values are seen to be systematically higher than the calculated ones. This is believed to be caused principally by neutrons leaking between the apex and the base of adjacent prisms. Attempts to stop these neutron leaks by adding cadmium strips placed between adjacent prisms have been only partly successful. Though this eliminated any undeflected trajectories, there remained additional smearing such that these leaks broaden the neutron spot vertically.

Error bars shown in Fig. 8 were obtained using the following propagation-of-errors formula:

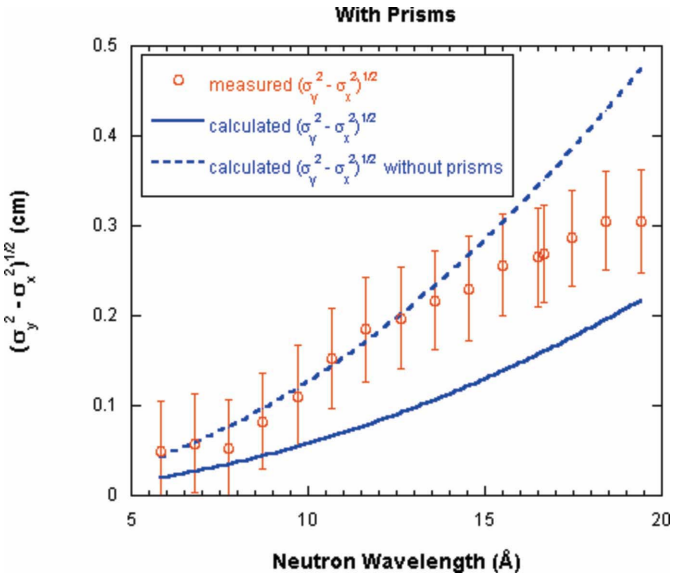

Figure 8
Variation of the variance of the neutron spot at the detector with wavelength. Statistical error bars have been included. Discrepancy between measured and calculated values is likely due to neutron leakage between adjacent prisms.

$$\delta[(\sigma_y^2 - \sigma_x^2)^{1/2}] = \left[\frac{\sigma_y^2\delta^2(\sigma_y) + \sigma_x^2\delta^2(\sigma_x)}{|\sigma_y^2 - \sigma_x^2|}\right]^{1/2}, \qquad (34)$$

where $\delta(\sigma_x)$, $\delta(\sigma_y)$ and $\delta[(\sigma_y^2 - \sigma_x^2)^{1/2}]$ are the errors in σ_x, in σ_y and in $(\sigma_y^2 - \sigma_x^2)^{1/2}$, respectively.

Fig. 9 shows the measured minimum vertical spot size $Y_{\min}$ plotted along with the calculated values. The difference $Y_{\min} - X_{\min}$ is expected to be given by $2|A - L_2C|\lambda^2(\Delta\lambda/\lambda)$. Here also, the neutron leakage between adjacent prisms is widening the vertical beam spot spread.

5.4. Discussion

Gravity causes the neutron beam to fall. This is seen as a lowering of the beam spot at the detector. Gravity also causes this spot to have an asymmetric oval shape. Prisms rectify for the neutron fall by deflecting the direct neutron beam upward. They also correct for the asymmetry of the neutron beam spot at the detector by correcting this oval shape back towards a circular one.

Analytical expressions for the spatial resolution including prisms have been presented. Effects have been analyzed for the variance of the resolution and for the minimum spot size. Both the measured variance and the minimum spot size were found to be larger than the calculated (predicted) values, likely due to neutron leakage between prisms.

6. Neutron beam current

Another figure of merit relevant to the performance of SANS instruments is the neutron beam current on the sample (*i.e.* number of neutrons per second reaching the sample aperture) as measured by the area detector; this is the total detector count rate summed up over the beam spot. Total detector count rates are included here for the three cases considered

before: empty-beam configuration, the use of focusing lenses and the use of gravity-correcting prisms. Fig. 10 summarizes the variation of the total detector count rate with $Y_{\min}$ for each case. Note that $Y_{\min}$ (not $X_{\min}$) is what determines $Q_{\min}$. The beam current depends on the ratio $(R_1R_2/L_1)^2$ which was the same in all three cases, and also on the neutron source spectrum. Each point corresponds to a different neutron wavelength (from 6 to 20 Å). No corrections have been made to account for the area detector efficiency or dead-time losses. These effects are strongly wavelength dependent and are outside of the scope of the present investigations.

Using neutron lenses lowers $Y_{\min}$ substantially without too much loss in neutron current, whereas using prisms is accompanied by neutron losses because of the prisms' low neutron transmission and due to the cadmium strips that were placed between adjacent prisms in order to minimize neutron leakage. The lowest $Y_{\min}$ obtained with the lenses (at 17.2 Å neutrons) has low neutron beam current (1252 counts s^{-1}). Note, however, that the contribution of the sample aperture to the variance of the resolution is reduced by a factor of $(2/3)(\Delta\lambda/\lambda)^2$. For the configuration of our measurements, this factor is about 1%! This means that, given appropriate sizes to the lenses, the sample aperture radius R_2 can be increased considerably without degrading the overall resolution. Consequently, the use of lenses with a large sample area can enable a great increase in beam current on the sample, with negligible effect on resolution. The prisms used here correct only partially for the effect of gravity. Had we used prisms that correct 'exactly' for the gravity effect, the prisms curve in Fig. 10 would have been vertical and shown no wavelength dependence.

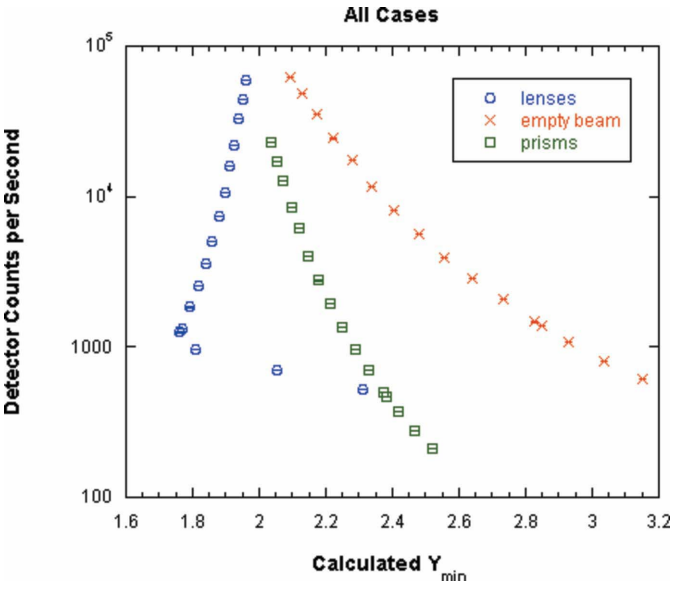

Figure 10
Variation of the total detector count rate within the neutron spot with the extent of the beam size in the vertical direction $Y_{\min}$. The three curves correspond to the three cases: (i) empty beam, (ii) with lenses and (iii) with prisms. Each data point corresponds to a different neutron wavelength. Vertical error bars are smaller than the plotting symbols.

7. Conclusions

Results of investigations of the SANS resolution when lenses and/or prisms are used have been presented. These include the theoretical calculations of the standard deviation (σ_Q) of the resolution function and of the minimum scattering variable ($Q_{\min}$). Neutron optics measurements including lenses and/or prisms have been compared with these predictions. Agreement is reasonable except in the case of prisms where neutron leakage between adjacent prisms add more smearing in the vertical direction.

In an effort to improve the performance of SANS instruments, focusing optics and gravity-correcting prisms can be added to the pre-sample collimation. Focusing lenses enhance the neutron current on the sample by allowing a widening of the sample aperture. They can also improve $Q_{\min}$ by tightening the beam spot at the detector. Correcting prisms deflect the falling neutron beam trajectory upward and correct the asymmetry of the neutron beam spot introduced by gravity effects.

Neutron lenses placed immediately before the sample aperture decrease the contribution of the sample aperture term to the spatial variance of the beam at the detector and the value of the minimum scattering vector, as well as enable an increase in the neutron current at the sample. The addition of prisms immediately before the sample aperture reduces the effect of gravity on the beam. They decrease the contribution of the wavelength term in the vertical direction to the spatial variance of the beam at the detector, and the value of the minimum scattering vector. Ideally one would like to have a combination of the two (both lenses and prisms) such that both effects (chromatic aberrations and gravity) could be reduced.

Many of the results presented here have not been reported before and others have been included here for the sake of completeness.

APPENDIX *A*
Focusing lens system: basic equations

The focal length for a set of N lenses of radius of curvature R and index of refraction n is given by

$$f = \frac{R}{2N(1-n)}. \tag{35}$$

The index of refraction n is related to the material atomic density ρ, neutron scattering length b_c, and neutron wavelength λ as

$$n = 1 - \frac{\rho b_c}{2\pi}\lambda^2. \tag{36}$$

Note that the focal length of the lens system varies inversely with the square of the neutron wavelength. The focal length is also related to the source-to-lenses distance L_1 and lenses-to-focal-point distance L_2 as

$$\frac{1}{f}=\frac{1}{L_1}+\frac{1}{L_2}. \tag{37}$$

Combining the above equations gives a relationship between the number N of lenses to use and the neutron wavelength λ. This condition is for an optimized instrument configuration where the detector is located at the focal spot:

$$\frac{\pi}{\rho b_c}\frac{R}{N\lambda^2}=\frac{L_1L_2}{L_1+L_2}. \tag{38}$$

For the single-crystal MgF_2 lenses used here, the factor $\rho b_c/\pi = 1.632\times10^{-6}$ Å^{-2}, so that

$$\frac{N\lambda^2}{R}\left(\frac{L_1L_2}{L_1+L_2}\right)=\frac{\pi}{\rho b_c}=6.13\times10^5\ \text{Å}^2. \tag{39}$$

MgF_2 lenses of radius of curvature R = 2.5 cm and height H = 2.5 cm were used. These lenses are thin at the center (0.5 mm thickness) in order to keep neutron transmission high. Source-to-sample and sample-to-detector distances corresponding to the SANS instrument configuration described earlier (L_1 = 16.14 m, L_2 = 13.19 m) give a focal length of

$$f=\left(\frac{L_1L_2}{L_1+L_2}\right)=726\ \text{cm}, \tag{40}$$

thereby yielding $N\lambda^2 = 2111$ Å^2. The use of seven consecutive lenses (N = 7) focuses neutrons of wavelength λ = 17.36 Å with a focal distance of 726 cm.

APPENDIX *B*
Prism system: basic equations

The equation for the parabolic neutron trajectory in the pre-sample collimation is given by:

$$y(z)=B\lambda^2 z(L_1-z),\qquad 0\le z\le L_1, \tag{41}$$

where

$$B=\frac{gm^2}{2h^2}=3.073\times10^{-9}\ \text{cm}^{-1}\ \text{Å}^{-2}. \tag{42}$$

The vertical component of the neutron trajectory slope $y'(z)$ is therefore

$$\begin{aligned} y'(z)&=B\lambda^2(L_1-2z), && 0\le z\le L_1\\ y'(L_1)&=-B\lambda^2L_1, && z=L_1. \end{aligned} \tag{43}$$

This neutron trajectory holds between the sample aperture and detector. The addition of a prism immediately before the sample aperture changes the neutron trajectory by introducing an upward deflection δ.

The slope of the neutron trajectory is changed to

$$y'(L_1)=-B\lambda^2L_1+\delta,\qquad z=L_1. \tag{44}$$

The neutron trajectory is therefore changed between the sample aperture and detector to the following form:

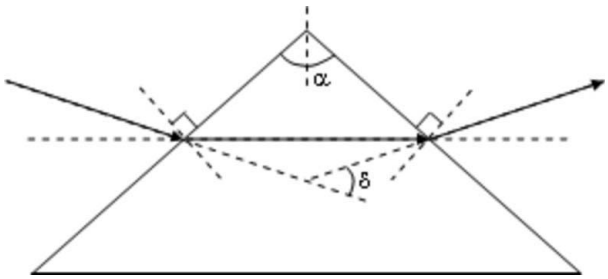

Figure 11
Schematics of a prism with the deflected neutron trajectory in the simple case of minimum deviation.

$$\begin{aligned} y(z)&=-B\lambda^2(z-L_1)^2\\ &\quad+[-B\lambda^2L_1+\delta](z-L_1), && L_1\le z\le L_1+L_2,\\ y(L_1+L_2)&=-B\lambda^2L_2(L_1+L_2)+\delta L_2, && z=L_1+L_2. \end{aligned} \tag{45}$$

The use of a prism with deflection angle $\delta = B\lambda^2(L_1 + L_2)$ would correct for the gravity effect exactly.

The 'prism equation' (in the case of minimum deflection where the refracted beam within the prism is parallel to the prism base as shown in Fig. 11) relates the total deflection angle δ, the prism angle α and the index of refraction n as follows:

$$n=\frac{\sin[(\alpha-\delta)/2]}{\sin(\alpha/2)}. \tag{46}$$

The deflection angle is expressed as

$$\delta=\alpha-2\sin^{-1}\left[n\sin\left(\frac{\alpha}{2}\right)\right]. \tag{47}$$

The wavelength dependence of the deflection angle enters through the index of refraction:

$$n=1-\frac{\rho b_c}{2\pi}\lambda^2. \tag{48}$$

For MgF_2 prisms, this becomes $n = 1 - 0.816\times10^{-6}\lambda^2$ (where λ is the neutron wavelength in Å).

In the small deviation-angle approximation, one can expand the prism formula assuming that $\delta \ll \alpha$ to obtain

$$\delta(\lambda)\simeq\left(\frac{\rho b_c}{\pi}\right)\tan\left(\frac{\alpha}{2}\right)\lambda^2=C\lambda^2. \tag{49}$$

This is an easier (approximate) expression used in order to obtain analytical results.

Certain commercial equipment, instruments, or materials are identified in this paper to foster understanding. Such identification does not imply recommendation or endorsement by the National Institute of Standards and Technology, nor does it imply that the materials or equipment identified are necessarily the best available for the purpose. This work is based upon activities supported in part by the National Science Foundation under Agreement No. DMR-0454672.

References

Choi, S. M., Barker, J. G., Glinka, C. J., Cheng, Y. T. & Gammel, P. L. (2000). *J. Appl. Cryst.* **33**, 793–796.
Eskildsen, M. R., Gammel, P. L., Isaacs, E. D., Detlefs, C., Mortensen, K. & Bishop, D. J. (1998). *Nature (London)*, **391**, 563–566.
Forgan, E. M. & Cubitt, R. (1998). *Neutron News*, **9**, 25–31.
Glinka, C. J., Barker, J. G., Hammouda, B., Krueger, S., Moyer, J. J. & Orts, W. J. (1998). *J. Appl. Cryst.* **31**, 430–445.
Mildner, D. F. R. & Carpenter, J. M. (1984). *J. Appl. Cryst.* **17**, 249–256.
Mildner, D. F. R., Hammouda, B. & Kline, S. R. (2005). *J. Appl. Cryst.* **38**, 979–987.
Sears, V.F. (1989). *Neutron Optics*. Oxford University Press.